Strain control of magnetism in graphene decorated by transition-metal atoms

Bing Huang,[1] Jaejun Yu,[1,2] and Su-Huai Wei[1]

[1]*National Renewable Energy Laboratory, 1617 Cole Boulevard, Golden, Colorado 80401, USA*

[2]*Center for Strongly Correlated Materials Research, Department of Physics and Astronomy, Seoul National University, Seoul 151-747, Korea*

(Received 17 May 2011; revised manuscript received 8 July 2011; published 5 August 2011)

We report a strain-controlled tuning of magnetism in graphene decorated by transition-metal (TM) atoms. Our first-principles calculations demonstrate that strain can lead to a sudden change in the magnetic configuration of a TM adatom and the local atomic structure in the surrounding graphene layer. A strong spin-dependent hybridization between TM d and graphene π orbital states, derived from the orbital selection rule of the local lattice symmetry, is responsible for the determination of the local electronic and magnetic structure. Our results indicate that the strain can be an effective way to control the magnetism of atomic-scale nanostructures, where the reliable control of their magnetic states is a key step for the future spintronic applications.

DOI: 10.1103/PhysRevB.84.075415 PACS number(s): 73.22.−f, 68.43.Bc, 73.20.Hb, 75.75.−c

I. INTRODUCTION

A reliable control of magnetic states is central to the use of magnetic nanostructures in future spintronics and quantum information devices.[1] Although it is shown that magnetism could be generally modulated by external magnetic[1–3] or electric[4] fields, it is desirable to find an alternative scheme to control the magnetism for various spintronic applications. Recently, graphene has gathered tremendous attention due to its unique electronic and mechanical properties for nanoscale electronics.[5] As a candidate material for spintronic devices, transition-metal-atom-decorated graphene (denoted as TM-graphene hereafter) has been studied extensively theoretically[6–9] and experimentally,[10–15] and it manifests some remarkable electronic and magnetic behaviors. Thus, developing a method to tune the magnetism of TM-graphene system is quite urgent for future spintronics applications.

Graphene is the thinnest material ever synthesized.[5] While it is one of the strongest materials ever measured experimentally,[16–19] it has been shown that it can sustain elastic deformations as large as 25%. In this paper, we predict that the strain is an effective way to control the magnetic properties of TM-graphene systems. As for the graphene layers, we considered a pristine graphene (PG) layer as well as graphene layers with defects of a single vacancy (SV) or a double vacancy (DV). It has been shown that vacancies in graphene can be created by electron irradiation[20,21] or ion bombardment.[22] Our results for the Mn-atom-decorated graphene demonstrate that the strain can induce a sudden change of the local atomic structure of graphene around a Mn atom and the spin state of the Mn atom. A strong spin-dependent hybridization between Mn d and graphene π orbital or dangling bond states is responsible for the determination of the local electronic and magnetic structure. We also showed that the strain-controlled magnetism in Mn-graphene is a general phenomenon happening in different TM-graphene systems.

II. COMPUTATIONAL METHODS AND MODELS

All the density-functional-theory (DFT) calculations were performed using VASP code.[23] We used the projector augmented wave (PAW) potentials and the generalized gradient approximation with the Perdew-Burk-Ernzerhof (PBE) functional to describe the core electrons and the exchange-correlation energy, respectively, which were proved to describe well the TM-graphene systems.[7,8,24,25] A 7×7 graphene supercell (98 C atoms) was used in our calculations, approaching the single defect limit (∼1% defect concentration). A 12×12 supercell was used to calculate the interaction of TM atoms on graphene. A Γ-centered $6 \times 6 \times 1$ **k**-point sampling was used for Brillouin-zone integration. Moreover GGA + U (with the onsite Hubbard U correction) calculations with $U = 5$ eV were performed to confirm the GGA results of the Mn-graphene system. We verified that both GGA and GGA + U results are consistent with each other.

III. RESULTS AND DISCUSSION

We take the case of Mn atom adsorption on graphene as a primary example to demonstrate the strain effect on the TM-graphene system. The calculated strain-dependent magnetic moments are shown in Fig. 1(a). A biaxial strain η is defined as $\eta = \Delta a/a$, where a is the lattice constant of free-standing graphene. A positive (negative) η means the TM-graphene system is under tension (compression). For PG without vacancies, the Mn atom prefers to stay at the hollow site (above the carbon hexagon center) of PG, and the total magnetic moment of Mn atom is 5.7 μ_B, indicating that Mn atom is in a high-spin state. The height and average bond length between Mn atom and its nearest C atoms are 2.09 Å and 2.54 Å, respectively, as shown in Figs. 1(b) and 1(c). The binding energy of Mn on PG is about 0.45 eV, as shown in Fig. 1(d). When a biaxial tensile strain η is applied for Mn-PG, interestingly, the magnetic ground state changes from high spin to low spin (∼3.1 μ_B) abruptly at the critical strain of $\eta = 0.05$, as shown in Fig. 1(a). Accompanying the magnetic transition, the height and average bond length between Mn atom and its nearest C atoms decrease sharply to 1.50 and 2.16 Å, respectively, as shown in Figs. 1(b) and 1(c). The binding energy of Mn atom of Mn-PG increases to 1.15 eV when $\eta = 0.05$. In contrast to the sharp transitions of spin states and local adsorption structures, the binding energy of Mn atom on PG increases continuously as a function of η, as shown in Fig. 1(d).

TM atoms on PG have low migration barriers so that it may be mobile at room temperature.[7,10,13,24,25] However, our climbing-image nudged-elastic-band calculations[26] show that the migration barrier for the Mn atom on PG increases from 0.36 eV to 0.89 eV under a tension of $\eta = 0.10$, giving rise to a decrease of more than eight orders of magnitude in the diffusion coefficient at room temperature, which implies that the migration can be suppressed significantly. It also indicates that an adequate variation of strain can be used to control the patterning of TM atoms on graphene. Furthermore, it is known that the mobility of the TM atom becomes markedly reduced in the presence of vacancies. For instance, the migration barriers for TM atoms on vacancies are larger than 3 eV.[7]

A similar magnetic transition between high-spin and low-spin states is also found for Mn atoms adsorbed near the SV sites in graphene (Mn-SV). Unlike the Mn-PG case, the unstrained Mn-SV is in a low-spin state with the magnetic moment of $\sim 3\ \mu_B$, as shown in Fig. 1(a). The local adsorption structures of the Mn atoms are shown in Fig. 1(e). The binding energy between Mn atom and vacancy is 6.4 eV, which is much larger than the Mn-PG case, indicating that the Mn-SV system is quite stable. This is in agreement with previous results.[7] Interestingly, a compression of $\eta = -0.04$ can convert the magnetic ground state from low spin ($\sim 3\ \mu_B$) to high spin ($\sim 5\ \mu_B$) for Mn-SV. Under compression, the graphene layer produces a spontaneous rippling with the formation of a C-C dimer bond near SV, as shown in Fig. 1(e). As results, the height and the average bond length between Mn and its nearest C atoms increase significantly under compression, which weakens the binding between Mn atom and vacancy. In general, we find that tensile (compressive) strain can enhance (reduce) the binding strength between TM atom and graphene [Fig. 1], which is consistent with experimental observation.[13]

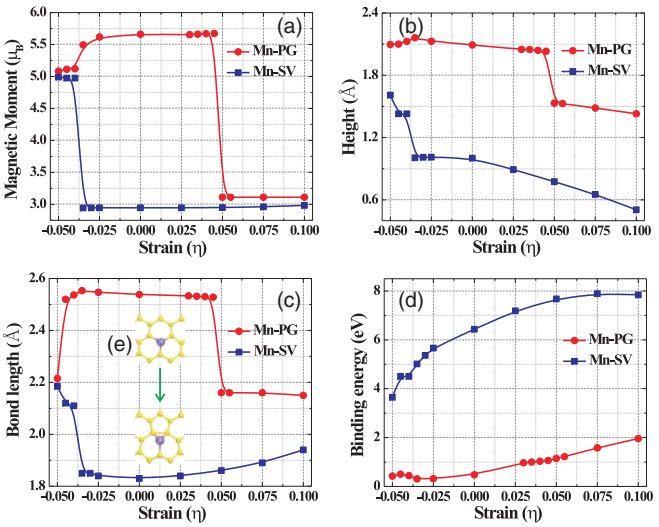

FIG. 1. (Color online) (a) Magnetic moments of Mn atoms adsorption on PG and defective graphene with a SV as a function of strain. (b) The heights between Mn atoms and the nearest C atoms as a function of strain for Mn-PG and Mn-SV systems. (c) The average bond lengths between Mn atoms and the nearest C atoms as a function of strain for Mn-PG and Mn-SV systems. (d) The binding energies of Mn atoms on graphene as a function of strain for Mn-PG and Mn-SV systems. (e) The local structure transition for Mn-SV system from $\eta = 0$ (up structure) to $\eta = -0.04$ (down structure).

It is interesting to observe that the electronic and magnetic structures of the Mn atom depend strongly on the strain of graphene layer, thereby leading to the strain-induced sudden change of the magnetic ground state. The strain affects the local geometry of carbon atoms around the Mn atom in two ways. It changes the height of Mn atom above the graphene layer and generates a ripple structure under the compressive strain. The change of the local environment, which determines the distance and symmetry of C p orbitals with respect to that of Mn d orbitals, can lead to a dramatic change in the magnetic d orbitals due to the strong spin-dependent hybridization between Mn d and C π orbital states.

The isolated Mn atom has $s^{1\uparrow}d^{5\uparrow}s^{1\downarrow}d^{0\downarrow}$ configuration with a spin exchange splitting around 4 eV. Since the Mn atom sits over the hollow site, the energy levels of $3d$ orbitals are broadened by the ligand field from the hybridization between Mn $3d$ and C p_π orbitals of the hexagon carbon atoms at the hollow site. Moreover, because the Mn spin-down energy level is above the graphene Fermi energy, one electron is transferred from Mn to the graphene layer. This is consistent with the observation that the magnetic configuration of the Mn atom in the Mn-PG case can be ascribed to $d^{5\uparrow}s^{1\uparrow}d^{0\downarrow}s^{0\downarrow}$ with the calculated magnetic moment of 5.7 μ_B shown in Fig. 1(a).

In the Mn-PG system, the local geometry of the Mn adatom above the center of the carbon hexagon has the C_{6v} symmetry. While Mn $d_{yz,zx}$ and d_{xy,x^2-y^2} orbitals belong to the E_1 and E_2 representations of C_{6v}, respectively, the p_π electrons near the Fermi level (E_F) can be also classified to A_1, E_1 (corresponding to the π state) and B_2, E_2 ($\pi^\star$ state). From the orbital selection rule, for example, the C $\pi^\star$ state couples most strongly with Mn d_{xy,x^2-y^2} orbitals because both of them belong to the same symmetry representation. Due to the exchange splitting of Mn d states, however, the spin-up Mn $d^\uparrow$ levels are close to the occupied C π states and the spin-down Mn $d^\downarrow$ levels are located near the unoccupied C $\pi^\star$ states. Consequently, the proximity between Mn $d^\downarrow$ and C $\pi^\star$ states makes the $d^\downarrow_{xy,x^2-y^2}$-$\pi^\star$ hybridization much stronger so that the unoccupied $d^\downarrow_{xy,x^2-y^2}$ state is pushed down close to E_F, as illustrated in Fig. 2(a).

When the graphene is under a tensile strain, the height of Mn atom lowers and the bond lengths between Mn and C atoms decrease [Figs. 1(b) and Figs. 1(c)]. At $\eta \sim 0.05$, the change becomes abrupt. This is because the reduced bond length with the lower height of Mn increases the hybridization strength between Mn d_{xy,x^2-y^2,z^2} and C $\pi^\star$ states so that the d_{xy,x^2-y^2} spin-down state becomes occupied. Since the Mn d_{xy,x^2-y^2} can hold two electrons, consequently, the occupation of the spin-down Mn d_{xy,x^2-y^2} orbital reduces the total magnetic moment and the exchange splitting as well. Therefore, the final magnetic configuration of Mn-PG for $\eta \geqslant 0.05$ becomes $d^{5\uparrow}d^{2\downarrow}$ with the magnetic moment of 3 μ_B.

In the case of Mn-SV, one has to consider the role of C dangling bond states arising from the carbon vacancy as illustrated in Figs. 2(c) and 2(d). At $\eta = 0.0$, the new structure can form without a significant lattice distortion. When a carbon

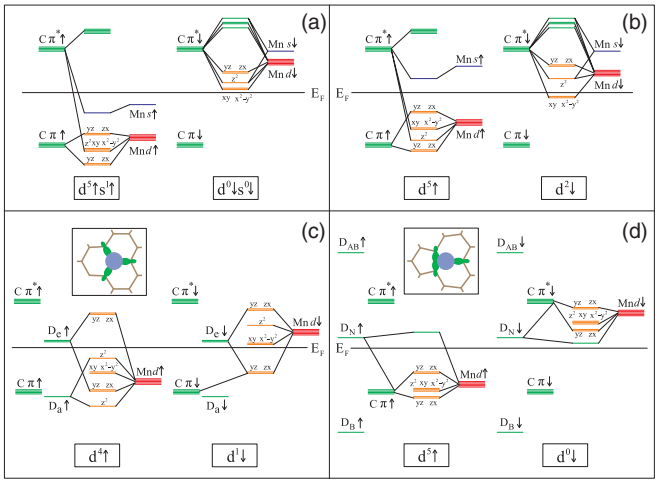

FIG. 2. (Color online) Schematic drawings of the energy diagrams of Mn atom and graphene electronic states near the Fermi level (E_F) for (a) Mn atom on PG under $\eta = 0$, (b) Mn atom on PG under $\eta = 0.05$, (c) Mn atom on graphene with SV under $\eta = 0$, and (d) Mn atom on graphene with SV under $\eta = -0.04$. The local electronic structure of graphene is represented by the occupied π and unoccupied $\pi^\star$ levels arising from C p_π bands, which touch at the K point in the orignal Brillouin zone of graphene. In (c), three dangling bond orbitals of C atoms near SV form one bonding state, labeled as D_a, and two degenerate nonbonding states, labeled as D_e. While the bonding D_a level is close to π, the nonbonding D_e level is located just above E_F. In (d), the distortion and formation of C-C pair gives rise to the bonding and antibonding states D_B and D_{AB}, which stay far away from the Fermi level, and one nonbonding dangling bond state D_N just above E_F.

vacancy is present within the graphene layer, the Mn atom is much closer to the graphene plane and the C-Mn bond length is much shorter. In this case, the main hybridization is between the Mn d state and the C dangling bond states from the neighboring C atoms. Similar to the case of Mn atom on PG, the coupling between the dangling bond states D_a and D_e and the Mn d states depends on the symmetries of the states. For example, the largest coupling occurs between Mn $d_{yz,zx}$ and C D_e states, whereas Mn d_{z^2} couples mostly to D_a. Here we have a similar spin-dependent hybridization effect due to the proximity of Mn $d^\uparrow$ to D_a and Mn $d^\downarrow$ to D_e levels, respectively. Due to the strong $d_{yz,zx}$-D_e coupling, the bonding-antibonding separation of the $d_{yz,zx}$-D_e hybrid states becomes much stronger than in the Mn-PG case, so that the antibonding Mn $d^\uparrow_{yz,zx}$-derived state becomes unoccupied, whereas the bonding Mn $d^\downarrow_{yz,zx}$-derived state is occupied as shown in Fig. 2(c). Although the occupied bonding states are doubly degenerate, their covalent character reduces the effective spin moment close to 1 μ_B. Thus, as illustrated in Fig. 2(c), the magnetic configuration for the case of Mn-SV without strain becomes $d^{4\uparrow}$ and $d^{1\downarrow}$ (the Mn s orbitals are in higher energy due to the charge transfer from Mn to graphene), which corresponds to the calculated magnetic moment of 3 μ_B shown in Fig. 1(a).

To achieve the high-spin state in Mn-SV, as we have learned from the Mn-PG case, we should increase the Mn-C distance to reduce the hybridization between the Mn d and C p_π state. Ironically, this should be done by compressive strain. Indeed, we find that for $\eta \leqslant -0.04$, the height of Mn increases drastically, and therefore so the Mn-C bond length increases as shown in Fig. 1(c). Moreover, the graphene layer around the SV region becomes strongly rippled, and two of the three carbon atoms around the vacancy site form a pair [Figs. 1(e) and Figs. 2(d)]. The C dangling bond states now become D_B, D_N, and D_{AB} [Fig. 2(d)]. Because of the elongated structure, the hybridization between the D_N and Mn d orbitals becomes much reduced in the rippled structure so that the Mn atom maintains its $d^{5\uparrow}d^{0\downarrow}$ configuration with the minimal d-level broadening for both spin-up and spin-down channels. Therefore, the spin transition of Mn-SV system indicates that the rippled graphene structures (induced by compression) play an important role in the spin transition from low-spin to high-spin state. It is quite encouraging to see that the rippling of graphene layers already can be controlled by substrates or thermal expansion in experiments.[5,19]

The strain control of the magnetism generally exists for almost all the TM atoms from Sc to Zn on graphene, not just the Mn atom on graphene. The range of magnetic moments of TM-graphene systems under realistic strain $-0.05 \leqslant \eta \leqslant 0.10$ is shown in Fig. 3. The transition of magnetic states for TM-PG systems under strain could be either continuous (e.g., V, Ti, and Cr) or abrupt (e.g., Sc, Mn, Fe, and Cu), as shown in Fig. 3(a), which is mainly due to different strain-dependent ligand splitting and hybridization. Interestingly, strain can also control the adsorption sites of TM atom, for example, the adsorption site of Cu (Sc and Fe) on graphene converts from

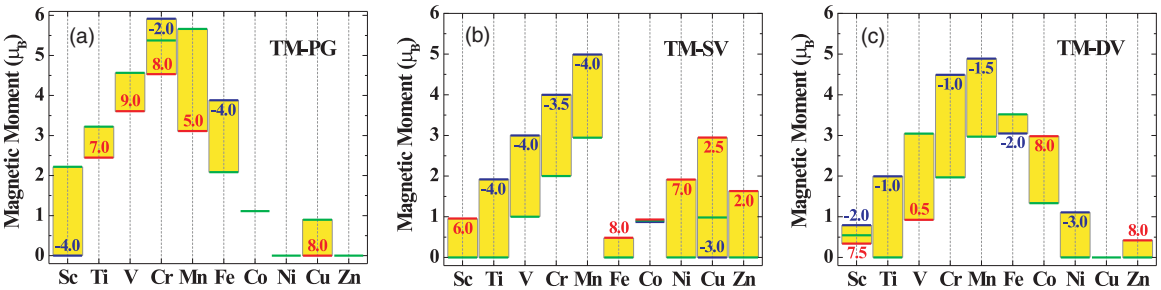

FIG. 3. (Color online) The range of magnetic moments of TM atoms adsorption on graphene (a) without vacancy, (b) with SV, (c) with DV under $-0.05 \leqslant \eta \leqslant 0.10$. The intrinsic magnetic moments of TM-graphene without strain are shown as green lines, while the maximum and minimum magnetic moments of TM-graphene caused by compressive (or tensible) strain (in unit of %) are shown by blue (or red) line.

C-C bridge (hollow) site to hollow (C-C bridge) site at $\eta \geqslant 0.08$ ($\eta \leqslant -0.04$).

The spin transition is even more remarkable in the TM-SV cases, as shown in Fig. 3(b). For example, compressive strains of −0.04, −0.04, and −0.035 could transfer Ti-, V-, and Cr-SVs from low-spin to high-spin states, respectively, similar to Mn-SV. Tensile strains of 0.025, 0.06, and 0.07 could transfer Cu-, Sc-, and Ni-SVs from low-spin to high-spin states, respectively. It should be noticed that at least 66% (50%) of total magnetic moments of the Cu-SV (Ni-SV) system origins from the nearest C atoms around vacancy. We have also studied the cases of TM-DV, since the stability of TM atoms adsorbed on DV is comparable to that of SV.[7] The spin transition in the TM-DV system is similar to that of TM-SV but with a smaller critical η for spin transition, as shown in Fig. 3(c). Particularly, compressive strains of −0.01, −0.01, and −0.015 could convert the spin states of Ti-, Cr-, and Mn-DV from low spin to high spin, respectively. Surprisingly, a very small tension of 0.005 could transfer V-DV from a high-spin to a low-spin state.

IV. SUMMARY

In conclusion, a concept of controlling the magnetism of TM-graphene by simply using a strain is reported. Our calculations demonstrate that the strain-induced change of the local atomic structure of graphene around a TM atom makes a dramatic effect on the spin state of the TM atom. A strong spin-dependent hybridization between TM d and graphene p orbital states, derived from the orbital selection of the local lattice symmetry, is responsible for the determination of the local electronic and magnetic structure. Our results indicate that the strain is available to control the magnetism of nanoscale materials for spintronics.

ACKNOWLEDGMENTS

The work at NREL was supported by the US Department of Energy under Contract No. DE-AC36-08GO28308. J.Y. acknowledges the support by the National Research Foundation of Korea through the ARP (No. R17-2008-033-01000-0).

[1] S. A. Wolf, D. D. Awschalom, R. A. Buhrman, J. M. Daughton, S. von Molnar, M. L. Roukes, A. Y. Chtchelkanova, and D. M. Treger, Science **294**, 1488 (2001).
[2] O. Kahn and C. J. Martinez, Science **279**, 44 (1998).
[3] C. F. Hirjibehedin, C. P. Lutz, and A. J. Heinrich, Science **312**, 1021 (2006).
[4] M. Weisheit, S. Fahler, A. Marty, Y. Souche, C. Poinsignon, and D. Givord, Science **315**, 349 (2007).
[5] A. K. Geim, Science **324**, 1530 (2009).
[6] B. Uchoa, V. N. Kotov, N. M. R. Peres, and A. H. Castro Neto, Phys. Rev. Lett. **101**, 026805 (2008).
[7] A. V. Krasheninnikov, P. O. Lehtinen, A. S. Foster, P. Pyykko, and R. M. Nieminen, Phys. Rev. Lett. **102**, 126807 (2009).
[8] E. J. G. Santos, A. Ayuela, and D. Sanchez-Portal, New J. Phys. **12**, 053012 (2010).
[9] B. Uchoa, T. G. Rappoport, and A. H. Castro Neto, Phys. Rev. Lett. **106**, 016801 (2011).
[10] Y. Gan, L. Sun, and F. Banhart, Small **4**, 587 (2008).
[11] K. Pi, K. M. McCreary, W. Bao, W. Han, Y. F. Chiang, Y. Li, S.-W. Tsai, C. N. Lau, and R. K. Kawakami, Phys. Rev. B **80**, 075406 (2009).
[12] V. W. Brar, R. Decker, H. Solowan, Y. Wang, L. Maserati, K. T. Chan, H. Lee, C. Girit, A. Zettl, S. G. Louie, M. L. Cohen, and M. F. Crommie, Nature Phys. **7**, 43 (2010).
[13] O. Cretu, A. V. Krasheninnikov, J. A. Rodriguez-Manzo, L. Sun, R. M. Nieminen, and F. Banhart, Phys. Rev. Lett. **105**, 196102 (2010).
[14] J. A. Rodriguez-Manzo, O. Cretu, and F. Banhart, ACS Nano **4**, 3422 (2010).
[15] R. Zan, U. Bangert, Q. Ramasse, and K. S. Novoselov, Nano Lett. **11**, 1087 (2011).
[16] C. Lee, X. Wei, J. W. Kysar, and J. Hone, Science **321**, 385 (2008).
[17] K. S. Kim, Y. Zhao, H. Jang, S. Y. Lee, J. M. Kim, K. S. Kim, J. Ahn, P. Kim, J. Choi, and B. Hong, Nature (London) **457**, 706 (2009).
[18] N. Levy, S. A. Burke, K. L. Meaker, M. Panlasigui, A. Zettl, F. Guinea, A. H. Castro Neto, and M. F. Crommie, Science **329**, 544 (2010).
[19] W. Bao, F. Miao, Z. Chen, H. Zhang, W. Jang, C. Dames, and C. N. Lau, Nature Nanotech. **4**, 562 (2009).
[20] A. Hashimoto, K. Suenaga, A. Gloter, K. Urita, and S. Iijima, Nature (London) **430**, 870 (2004).
[21] A. V. Krasheninnikov and F. Banhart, Nat. Mater. **6**, 723 (2007).
[22] M. M. Ugeda, I. Brihuega, F. Guinea, and J. M. Gomez-Rodriguez, Phys. Rev. Lett. **104**, 096804 (2010).
[23] G. Kresse and J. Furthmüller, Comput. Mater. Sci. **6**, 15 (1996).
[24] K. T. Chan, J. B. Neaton, and M. L. Cohen, Phys. Rev. B **77**, 235430 (2008).
[25] H. Sevincli, M. Topsakal, E. Durgun, and S. Ciraci, Phys. Rev. B **77**, 195434 (2008).
[26] G. Henkelman, B. P. Uberuaga, and H. Jonsson, J. Chem. Phys. **113**, 9901 (2000).